Response to the comments of Anonymous Referee #1

Li et al. present the evaluation of a custom ECCC-OFR design by performing characterization studies that included measurements of size-dependent particle transmission efficiency and yields of SOA generated from OH oxidation of α-pinene and C7, C10, and C12 n-alkanes in the presence and absence of ammonium sulfate seeds. Results are compared to those obtained with other OFRs and environmental chambers. Unlike in previous OFR studies, alkane-generated SOA did not exhibit a decrease in yield at high OH exposure due to fragmentation reactions. The ECCC-OFR is then used to investigate the SOA formation potential following OH oxidation of materials obtained from oil sands operations in Alberta. Cyclic alkanes are implicated as the most important class of precursors in the oil sands samples. Overall, the manuscript reads well. Given the emergence of OFRs as a technique to characterize SOA formation, and the application of the ECCC-OFR to study the aging of environmentally-relevant VOC mixtures that are emitted during oil sands extraction activities, I would support eventual publication of this manuscript in ACP. However, in its current form, I have reservations about assumptions that are made regarding laminar flow behavior, reduced wall losses compared to other OFRs, and SOA yield calculations that are heavily reliant on offline measurements of SOA precursor concentrations. In my opinion these assumptions are not adequately justified based on the current information that is given, and any related conclusions made about ECCC-OFR performance compared to other OFRs are uncertain at present.

Response: We thank Anonymous Referee #1 for the review and the positive evaluation of our manuscript. We have fully considered the comments, responded to these comments below in blue text and made the associated revisions to the manuscript as shown in red text. The response and changes are listed below.

General Comments

1. Recent OFR applications and modeling studies have demonstrated the utility of 185 nm radiation in OFRs due to ease of use in the field and due to additional HO_x generation via $H_2O + h\nu(185) \rightarrow H + OH$, $H + O_2 \rightarrow HO_2$. Here, the authors specifically mention that they chose to use mercury lamps that exclude the 185 nm emission line. Please explain the reasons for this choice.

Response: The lamps are located outside of the fused quartz reactor, and the transmittance of 185 nm UV light through fused quartz is very small, which limits the application of 185 nm UV lamps in our OFR. We calculate that only ~5% of the 185 nm light can be transmitted through the fused quartz wall; hence, 185 nm lamps were not used. Placing the lamps on the inside of the OFR to avoid this problem would have introduced additional surface areas and turbulence, thus negating some of the other advantages of this OFR, such as reduced wall loses. In addition, interior 185 nm lights would have made temperature control difficult. Exterior lamps allow the temperature of the OFR to be maintained accurately.

To address these points we added the following text in the revised manuscript (P4, L18-23):

"Recent OFR applications and modeling studies have demonstrated the utility of 185 nm radiation in OFRs due to ease of use in the field and due to additional OH and HO_2 generation (Li et al., 2015;Palm et al., 2016). However, the fused quartz tubes of ECCC-OFR limit the application of such lamps due to the low transmittance of 185 nm radiation (~5%), and placement of lamps on the interior of the OFR are likely to increase turbulence and wall losses within the OFR, and limit overall OFR temperature control. Consequently, 254 nm radiation lamps were used."

2. The actinic flux at 254 nm is an important OFR characteristic that, unless I missed it, was never measured or calculated. It would be worthwhile to calculate this value and compare to the other OFR designs that are mentioned. For example, a possibility that is never discussed is whether potential SOA photolysis at 254 nm (which is more potentially important at high UV intensity and OH exposure) might be less important in the ECCC-OFR than in the PAM OFR due to lower actinic flux. I am not necessarily convinced that this is the case, but it should be briefly discussed and ruled out if not applicable. The preferable method to quantify the actinic flux would be to photolyze a compound with known absorption cross section at 254 nm as a function of lamp voltage. At the least, I think the maximum actinic flux inside the ECCC-OFR could be estimated from the wattage of the UV lamps at full output normalized by the internal surface area, with the caveat that I am not to what extent the mirrored enclosure referred to on P4, L14-15 would influence this calculation.

Response: We have now determined the maximum photon flux (with 4 lamps on) based upon the measured ozone decay and OH exposure (without precursor injection) combined with a photochemical box model characterizing radical chemistry in OFRs (Oxidation Flow Reactor Exposure Estimator 3.1) (Li et al., 2015;Peng et al., 2018). The input photon flux of the model was adjusted to match the measured ozone decay and OH exposure, which resulted in a maximum photon flux estimate of ~1.9×10^{16} photons cm^{-2} s^{-1}. This photon flux is similar to the PEAR OFR (2.3×10^{16} photons cm^{-2} s^{-1}) using the same estimation method (Ihalainen et al., 2019), and about three times that reported for the PAM (6.4×10^{15} photons cm^{-2} s^{-1}) (Lambe et al., 2017). Consequently, we can rule out the possibility of lower SOA photolysis in the ECCC-OFR as the reason for the higher yields in the ECCC-OFR compared to the PAM OFR.

The above content has been added to the revised manuscript (P4, L23-29).

3. In the ECCC-OFR, the authors state that an inlet with a cone angle of 30˚ is used to "minimize the establishment of jetting and recirculation in the OFR", which is steeper than the 15˚ cone angle used by Huang et al. (2017) and the 14˚ cone angle used by Ihalainen et al. (2019). Whereas both of those studies employed CFD simulations to optimize their OFR design, there are no corresponding simulations of the ECCC-OFR fluid dynamics that support the 30˚ cone angle used here. Please provide supporting calculations and/or residence time distribution measurements supporting the claim that laminar flow is achieved and jetting/recirculation is not present when using a 30˚ cone angle.

Response: The reviewer is not comparing the same angles in the above comment. The cone angle mentioned in our paper (i.e., 30˚) and Huang et al. (2017) is the full cone angle, while Ihalainen et al. (2019) reported the half cone angle. If the same angles are compared, then the half cone angles for the various OFRs are: 7.5˚ for Huang et al. (2017), 14˚ for Ihalainen et al. (2019), and 15˚ for the ECCC-OFR of this study. Hence, the cone angle of ECCC-OFR is very similar to that of the PEAR OFR (Ihalainen et al., 2019). This cone angle comparison was added to Sect. S1 of the Supplement.

To assess the near laminar flow of the ECCC-OFR, computational fluid dynamics (CFD) simulations were performed using ANSYS Fluent software (Version 2019 R2) in three dimensions to characterize the flow field inside the ECCC-OFR. Hybrid tetrahedral–hexahedral mesh consisting of 5.7×10^5 computation cells were used. Turbulence was modeled using a realizable k-epsilon model. The simulation results are shown in Fig. S4. It is shown in Fig. S4a that the flow velocity distribution in the reactor is generally uniform. A high velocity is observed only near the inlet, but reduces to the average velocity in

the conical diffuser. The velocity distribution here indicates that jetting is much weaker in ECCC-OFR compared to PAM (Mitroo et al., 2018). Fig. S4b indicates that the flow field is quite good in ECCC-OFR, with a small recirculation zone, similar to previous studies using a conical diffusion inlet (Huang et al., 2017;Ihalainen et al., 2019), but much better than PAM (Mitroo et al., 2018). These CFD simulations were added to Sect. S2 of the Supplement.

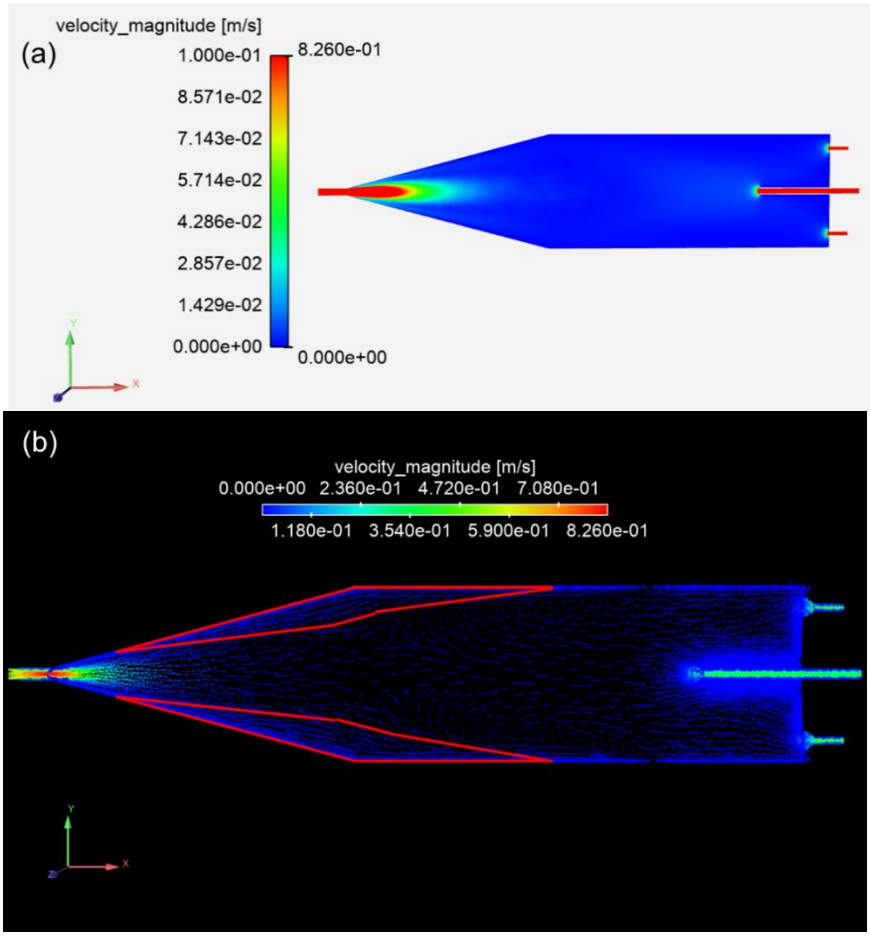

Figure S4. CFD simulation results: (a) velocity distribution; (b) vectors showing flow field. The red lines in (b) indicate the areas with recirculation.

4. The authors hypothesize that wall interactions are minor in the ECCC-OFR based on a calculation of the diffusion timescale (1400 sec) that is much longer than the residence time (120 sec) (P7, L1-8). Applying the same calculation to the PAM OFR, which has an inner radius of 10.2 cm, yields a diffusion timescale of 1474 sec. Given similar residence times and diffusion timescales, this line of reasoning would suggest similar wall interactions between the two systems. However, large-scale dispersion and recirculation inside OFRs (e.g. Lambe et al., 2011; Huang et al., 2017) complicates this sort of simple diffusion-based calculation. Later on (P9, L6-7), the authors speculate that higher SOA yields and less fragmentation are observed in the ECCC-OFR because of reduced wall interactions compared to other OFRs. This might be the case, but it is not supported by the logic presented above. This conclusion should be supported with a corresponding residence time distribution measurement and comparison to the RTD expected for ideal laminar flow, which was not performed here (P7, L9). In my opinion this is a critical

oversight that should be addressed. Additionally, I suggest measuring the yield of sulfuric acid generated from OH oxidation of SO_2 and comparing the result to other OFRs. Because sulfuric acid is not affected by photolysis or fragmentation, any difference in sulfuric acid yields between OFRs should be directly related to wall losses/interactions.

Response: Based upon the CFD simulation results above, we know that the flow field in ECCC-OFR is not perfectly ideal laminar flow, though it is significantly better than previous OFRs with a straight inlet, e.g., PAM (Mitroo et al., 2018). Hence, our assumption based on ideal laminar flow (using a diffusion timescale compared to the residence time to infer the gas-wall interactions) was removed in our revised paper (P7, L16-26).

The residence time distribution (RTD) was measured for ECCC-OFR and compared to ideal laminar flow in Fig. S5. The RTD was characterized by injecting a constant flow rate of CO_2 (10 s) into the OFR. The CO_2 concentration was then monitored from the sampling outlet of OFR with a CO_2 analyzer (Li-Cor LI-840A). The RTD was calculated from the differential CO_2 as a function of time elapsed since the start of injection. Fig. S5 indicates that the residence time associated with the CO_2 maximum intensity for the measured RTD and the ideal laminar flow RTD are in good agreement, and improved over the PAM and TPOT (Lambe et al., 2011). The shape of measured RTD before ~100 s is similar to the ideal laminar flow RTD, but slightly wider, which is likely due to dispersion. After ~100 s, the measured decrease in CO_2 is slower than for ideal laminar flow, which is likely due to recirculation in the OFR (Fig. S4).

This paragraph and associated figure were added to Sect. S2 of the Supplement.

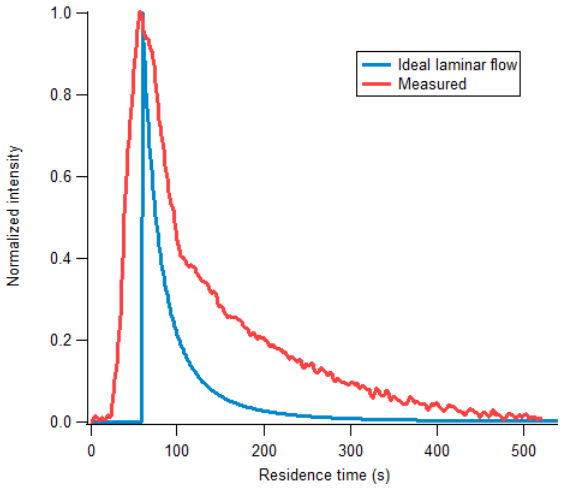

Figure S5. Residence time distribution (RTD) of CO_2 in ECCC-OFR compared to ideal laminar flow.

As suggested by the reviewer, the OH oxidation of SO_2 was performed in the ECCC-OFR. The SO_2 concentrations used were in the range of 24-63 ppb and the OH exposure was in the range of 3-10 $\times 10^{11}$ molec cm^{-3} s, which are similar to those used in a previous PAM study (Lambe et al., 2011). The yield of sulfuric acid ($Y_{H_2SO_4}$) was calculated using the mass fraction of H_2SO_4 in particles ($x_{H_2SO_4}$), the SMPS-measured particle volume ($V_{H_2SO_4 \cdot H_2O}$, nm^3 cm^{-3}), the density of the particles ($\rho_{H_2SO_4 \cdot H_2O}$, g cm^{-3}), and the measurement of the reacted SO_2 (ΔSO_2, ppb), using an approach which has been described in detail previously (Lambe et al., 2011):

$$Y_{H_2SO_4} = \frac{x_{H_2SO_4} \times V_{H_2SO_4 \cdot H_2O} \times \rho_{H_2SO_4 \cdot H_2O}}{3.95 \times \Delta SO_2}$$

The $x_{H_2SO_4}$ and $\rho_{H_2SO_4 \cdot H_2O}$ were estimated using the Extended Aerosol Inorganic Thermodynamic Model (E-AIM) I (http://www.aim.env.uea.ac.uk/aim/aim.php) (Carslaw et al., 1995). The dry yield of H_2SO_4 from OH oxidation of SO_2 is 3.95 μg m^{-3} per ppb SO_2 reacted (Lambe et al., 2011); hence $Y_{H_2SO_4}$ is expected to be 100% without wall losses. As shown in Fig. S6, the yield of sulfuric acid is 100±4% in this study, which is in agreement with the expected yield. The yield here is significantly higher than that obtained in previous OFR study using similar SO_2 concentrations and OH exposures (PAM and TPOT), which are mainly in the range of ~15%-50% (Lambe et al., 2011). This may be a result of lower wall losses in current OFR for gas-phase sulfuric acid and/or particles. Given that sulfuric acid is not impacted by photolysis or fragmentation, the result here suggest that wall losses/interactions within the ECCC-OFR are significantly lower than previous OFRs that utilize straight inlets (PAM and TPOT).

The above paragraph was added to the revised manuscript (P7, L27-33; P8, L1-3) and the Supplement (Sect. S5).

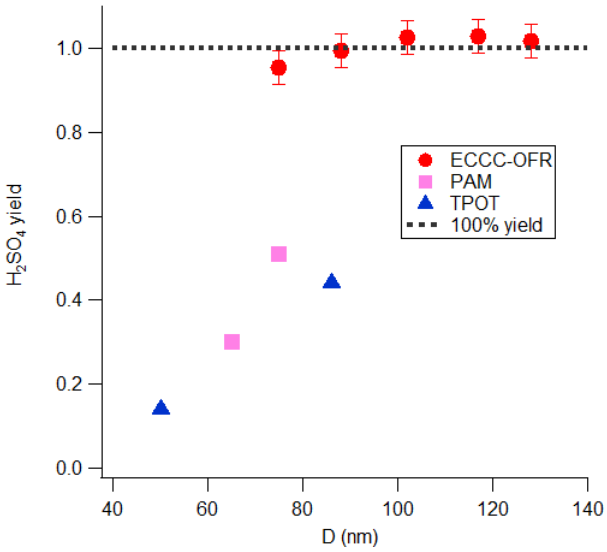

Figure S6. H_2SO_4 yields as a function of particle diameter in the ECCC-OFR and previous OFRs (Lambe et al., 2011).

Specific/Technical Comments

5. **P4, L16**: Please specify the O_3 mixing ratio (or range of O_3 mixing ratios) that was added to the OFR in these studies.

Response: The O_3 mixing ratio was ~12 ppm (now noted on P4, L17).

6. **P5, L5-7**: Because precursor concentrations were only obtained in offline measurements, how did the authors determine that the precursor concentrations remained constant and precise during the OFR experiments? As written, in the absence of other supporting/independent measurements this seems to be a major assumption and potential source of uncertainty in the SOA yield calculations.

Response: The THC concentration was measured before and after each experiment, and the difference was found to be less than 5%, representing a small uncertainty in the experiments. In addition, the precursor concentration was qualitatively checked during each experiment by repeating the same UV light intensity several times. For example, the UV lamp voltages were stepped from 120→50→60→120→70→80→120 etc... The absolute amount of SOA formed at the repeated light intensities varied by less than 5%, indicating that the THC precursor concentration was rather stable during experiments.

We have added the following text in the revised manuscript (P5, L22-24): "The THC concentration was measured before and after each experiment, resulting in differences of less than 5%. In addition, the magnitude of SOA formed for repeated experiments at the same light intensity varied by less than 5%, further indicating the stability of the precursor concentration over time."

7. **Figure 1 and Section 3.1.1.**: The Lambe et al. 2011 reference used a Pyrex chamber, where wall losses of charged particles are higher than chambers made of conductive materials due to charge buildup on nonconductive surfaces. A better reference/comparison here would be to use the data from Figure S1 of Karjaranen et al. (2016) which used an aluminum chamber with conductive coating. Their particle transmission data is shown below for reference. Please modify the discussion and figure accordingly.

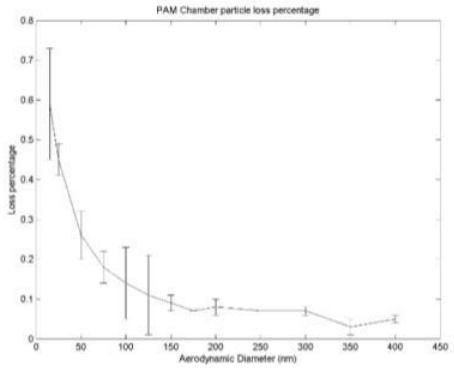

Figure S1. Primary particle losses in a similar PAM chamber that was used in the study.

Response: Particle transmission efficiencies from Karjalainen et al. (2016) and Ihalainen et al. (2019) were added in Figure 1 (now Figure 2).

The corresponding discussion was changed in the revised manuscript (P6, L28-31; P7, L1-2):

"The P_{trans} of other OFRs are also shown in Fig. 2 for comparison and indicates that the current P_{trans} is similar to that of the TSAR (TUT Secondary Aerosol Reactor) (Simonen et al., 2017) and PEAR (Ihalainen et al., 2019), likely due to the similarity in design (i.e., cone shaped inlet and sampling from the center-line, see Sect. S1 in Supplement). Conversely, the P_{trans} of the TPOT (Toronto Photo-Oxidation Tube), PAM-glass (PAM reactor with glass wall) (Lambe et al., 2011), PAM-metal (PAM reactor with metal wall) (Karjalainen et al., 2016), and CPOT (Caltech Photooxidation Flow Tube) (Huang et al., 2017) are 15-85%, 20-60%, 10-25%, and 20-45% lower respectively than the ECCC-OFR across a range of particle sizes."

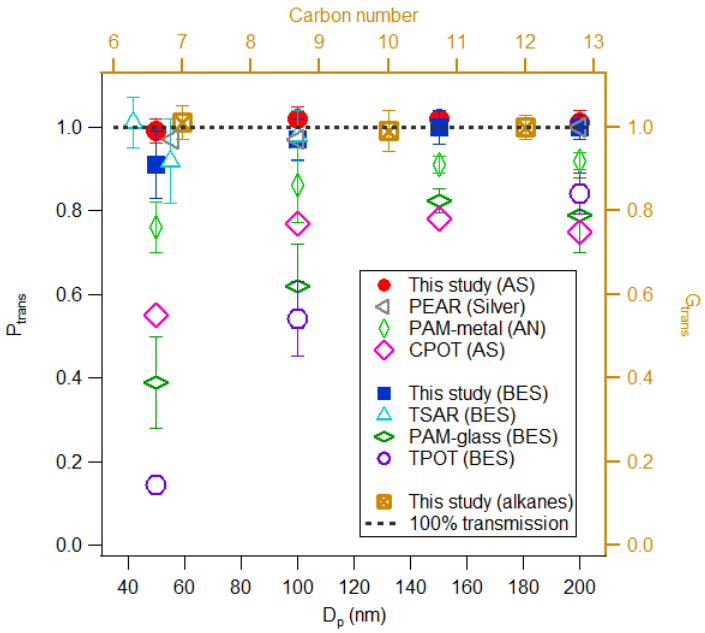

Figure 2. Particle (left and bottom axis) and gas (right and top axis) transmission efficiencies (P_{trans} and G_{trans}) for the ECCC-OFR. Particle transmission efficiencies of other OFRs are shown for comparison: PAM-glass and TPOT (Lambe et al., 2011), PAM-metal (Karjalainen et al., 2016), TSAR (Simonen et al., 2017), CPOT (Huang et al., 2017) and PEAR (Ihalainen et al., 2019).

8. **P15, L7**: The authors state: "all future OFR experiments should be conducted with seed particles to obtain more relevant qualitative and quantitative data." I suggest making this statement in the specific context of laboratory SOA yield studies, as not all OFR experiments are intended to measure SOA yields and because addition of seed particles in ambient OFR experiments is not necessarily always desirable or practical.

Response: The line in has been revised as: "This suggests that future laboratory OFR experiments studying SOA yields should be conducted with seed particles to obtain more relevant qualitative and quantitative data." (P15, L23-24).

9. **P11, L30 and Figure 4c**: Lambe et al. (2012) do not report absolute SOA yields from OH oxidation of diesel fuel and crude oil so it is unclear where this statement originates from.

Response: The carbon and oxygen yields of diesel fuel and crude oil in Figure 4c (now is Figure 5b) are what are referred to as the "normalized yields". We do not use the absolute yields here as we only compare the relative change of yields (relative to the maximum yield) among different precursors.

We changed the figure caption to reflect this: "…normalized Y_C and Y_O for diesel and crude oil…" (P24, L6).

10. **Figure 1**: It may be worth adding particle transmission data from Ihalainen et al. (2019) to this figure. Also, how much passivation time is required to obtain 100% transmission efficiency of C7, C10 and C12 alkanes, and at what mixing ratios are they introduced to the ECCC-OFR?

Response: Particle transmission data from Ihalainen et al. (2019) are now added to Figure 1 (now Figure 2), see above response to Comment 7 for details.

The passivation time was 5-10 min, and the mixing ratio was 300-500 ppb for these alkanes (now noted in P7, L10-11).

11. **Figure 3**: I think this could be moved to the Supplement.

Response: This figure provides important information about the LVOC fates in ECCC-OFR, and can help to better understand the final corrected SOA yields from OS precursors. Hence, we have decided to keep it in the main manuscript.

12. **Figures 4-6 and related text**: I suggest a reorganization to improve clarity and flow. First, move the current Figure 5 to the Supplement or to Methods. Second, combine the current Figure 6a with the current Figures 4a and 4b into a single 3-panel figure. Third, move the current Figure 4d into a separate figure and place between current Figures 4 and 6.

Response: Figure 5 is now Figure 1 and is described in Methods (P5, L27-28): "The chromatogram and the derived VD of the OS-related precursors are shown in Fig. S2 and Fig. 1 and discussed in detail in Sect. S4 of the Supplement."

Figures 1-3 are now Figures 2-4; Figure 6a is now moved into Figure 5 as Figure 5d; Figure 4d is now Figure 6; Figure 6b is now Figure 7.

The corresponding text is revised to match the Figure numbers above.

References

Carslaw, K. S., Clegg, S. L., and Brimblecombe, P.: A Thermodynamic Model of the System HCl-HNO3-H2SO4-H2O, Including Solubilities of HBr, from <200 to 328 K, The Journal of Physical Chemistry, 99, 11557-11574, 10.1021/j100029a039, 1995.

Huang, Y., Coggon, M. M., Zhao, R., Lignell, H., Bauer, M. U., Flagan, R. C., and Seinfeld, J. H.: The Caltech Photooxidation Flow Tube reactor: design, fluid dynamics and characterization, Atmospheric Measurement Techniques, 10, 839-867, 10.5194/amt-10-839-2017, 2017.

Ihalainen, M., Tiitta, P., Czech, H., Yli-Pirilä, P., Hartikainen, A., Kortelainen, M., Tissari, J., Stengel, B., Sklorz, M., Suhonen, H., Lamberg, H., Leskinen, A., Kiendler-Scharr, A., Harndorf, H., Zimmermann, R., Jokiniemi, J., and Sippula, O.: A novel high-volume Photochemical Emission Aging flow tube Reactor (PEAR), Aerosol Science and Technology, 53, 276-294, 10.1080/02786826.2018.1559918, 2019.

Karjalainen, P., Timonen, H., Saukko, E., Kuuluvainen, H., Saarikoski, S., Aakko-Saksa, P., Murtonen, T., Bloss, M., Dal Maso, M., Simonen, P., Ahlberg, E., Svenningsson, B., Brune, W. H., Hillamo, R., Keskinen, J., and Rönkkö, T.: Time-resolved characterization of primary particle emissions and secondary particle formation from a modern gasoline passenger car, Atmospheric Chemistry and Physics, 16, 8559-8570, 10.5194/acp-16-8559-2016, 2016.

Lambe, A., Massoli, P., Zhang, X., Canagaratna, M., Nowak, J., Daube, C., Yan, C., Nie, W., Onasch, T., Jayne, J., Kolb, C., Davidovits, P., Worsnop, D., and Brune, W.: Controlled nitric oxide production via O(¹D) + N₂O reactions for use in oxidation

flow reactor studies, Atmospheric Measurement Techniques, 10, 2283-2298, 10.5194/amt-10-2283-2017, 2017.

Lambe, A. T., Ahern, A. T., Williams, L. R., Slowik, J. G., Wong, J. P. S., Abbatt, J. P. D., Brune, W. H., Ng, N. L., Wright, J. P., Croasdale, D. R., Worsnop, D. R., Davidovits, P., and Onasch, T. B.: Characterization of aerosol photooxidation flow reactors: heterogeneous oxidation, secondary organic aerosol formation and cloud condensation nuclei activity measurements, Atmospheric Measurement Techniques, 4, 445-461, 10.5194/amt-4-445-2011, 2011.

Li, R., Palm, B. B., Ortega, A. M., Hlywiak, J., Hu, W., Peng, Z., Day, D. A., Knote, C., Brune, W. H., de Gouw, J. A., and Jimenez, J. L.: Modeling the radical chemistry in an oxidation flow reactor: radical formation and recycling, sensitivities, and the OH exposure estimation equation, The journal of physical chemistry. A, 119, 4418-4432, 10.1021/jp509534k, 2015.

Mitroo, D., Sun, Y., Combest, D. P., Kumar, P., and Williams, B. J.: Assessing the degree of plug flow in oxidation flow reactors (OFRs): a study on a potential aerosol mass (PAM) reactor, Atmospheric Measurement Techniques, 11, 1741-1756, 10.5194/amt-11-1741-2018, 2018.

Palm, B. B., Campuzano-Jost, P., Ortega, A. M., Day, D. A., Kaser, L., Jud, W., Karl, T., Hansel, A., Hunter, J. F., Cross, E. S., Kroll, J. H., Peng, Z., Brune, W. H., and Jimenez, J. L.: In situ secondary organic aerosol formation from ambient pine forest air using an oxidation flow reactor, Atmospheric Chemistry and Physics, 16, 2943-2970, 10.5194/acp-16-2943-2016, 2016.

Peng, Z., Palm, B. B., Day, D. A., Talukdar, R. K., Hu, W., Lambe, A. T., Brune, W. H., and Jimenez, J. L.: Model Evaluation of New Techniques for Maintaining High-NO Conditions in Oxidation Flow Reactors for the Study of OH-Initiated Atmospheric Chemistry, ACS Earth and Space Chemistry, 2, 72-86, 10.1021/acsearthspacechem.7b00070, 2018.

Simonen, P., Saukko, E., Karjalainen, P., Timonen, H., Bloss, M., Aakko-Saksa, P., Rönkkö, T., Keskinen, J., and Dal Maso, M.: A new oxidation flow reactor for measuring secondary aerosol formation of rapidly changing emission sources, Atmospheric Measurement Techniques, 10, 1519-1537, 10.5194/amt-10-1519-2017, 2017.